Journal of Thermal Analysis and Calorimetry (2025) 150:10401–10412
https://doi.org/10.1007/s10973-025-14394-3

Thermal performance evaluation of pure PDMS and PDMS composites heat exchangers

Reinaldo Souza[1,2] · Glauco Nobrega[1,3] · Inês S. Afonso[1,3,4] · José Pereira[2] · Elaine Cardoso[5,6] · Filipe Marques[1] · Cândida Vilarinho[1] · Ana Moita[2,7] · Rui A. Lima[1,8,9]

Received: 25 November 2024 / Accepted: 6 May 2025 / Published online: 10 June 2025

Abstract

This study investigates the heat transfer performance of three types of heat exchangers: one made of pure polydimethylsiloxane (PDMS), another incorporating recycled graphite (PDMS + Graphite 30 mass%), and a third using commercial aluminium nanoparticles (PDMS + Aluminium 30 mass%). Thermal performance was evaluated by measuring the thermal conductivity of the materials, analysing experimental convection tests with deionized water in a single-phase regime and using a thermal camera to obtain temperature profiles of the different surfaces. The results revealed that the composites formed with PDMS matrix and recycled graphite showed elevated thermal conductivity, approximately 2.7 times higher than pure PDMS. The heat transfer coefficient performance was 2.5 times superior to that of the heat exchanger made with commercial aluminium nanoparticles and up to 5 times higher compared to pure PDMS. The thermal analysis highlighted the benefits of the composites, showing a more uniform temperature distribution both in the serpentine channel and along the sides of the PDMS. The study aimed to provide an economical alternative that also contributes to waste valorisation. These findings validate the effectiveness of recycled particles in improving heat transfer performance in heat exchangers made from a combination of PDMS matrix and recycled, economical materials.

Keywords PDMS heat exchanger · Polymeric matrix composites · Waste particle · Thermal conductivity · Heat transfer

List of symbols

A_{eff}	Effective area (m^2)
c_p	Specific heat capacity ($J\ kg^{-1}\ K^{-1}$)
D_h	Hydraulic diameter (mm)
f	Fully developed friction factor (–)
f_{app}	Apparent friction factor (–)
G	Function of the channel aspect ratio (–)
h	Heat transfer coefficient ($W\ m^{-2}\ K^{-1}$)
H_{ch}	Channel height (mm)
k	Thermal conductivity ($W\ m^{-1}\ K^{-1}$)
L	Length of the test section channel (m)
L^+	Hydraulic channel length (–)
$\dot{m}$	Mass flow rate ($kg\ s^{-1}$)
Nu	Nusselt number (–)
Pr	Prandtl number (–)
Δp	Pressure drop (Pa)

✉ Reinaldo Souza
reinaldo.souza@tecnico.ulisboa.pt

1 Mechanical Engineering Department, Mechanical Engineering and Resource Sustainability Center (MEtRICs), University of Minho, Campus de Azurém, 4800-058 Guimarães, Portugal

2 IN+, Center for Innovation, Technology and Policy Research, Instituto Superior Técnico, Universidade de Lisboa, Av. Rovisco Pais, 1049-001 Lisbon, Portugal

3 Centro de Investigação de Montanha (CIMO), Campus de Santa Apolónia, Instituto Politécnico de Bragança, 5300-253 Braganca, Portugal

4 International Iberian Nanotechnology Laboratory, 4715-330 Braga, Portugal

5 School of Engineering, UNESP - São Paulo State University, Av. Brasil, 56, Ilha Solteira, SP 15385-000, Brazil

6 School of Engineering, UNESP - São Paulo State University, São João da Boa Vista, Brazil

7 CINAMIL—Centro de Investigação Desenvolvimento e Inovação da Academia Militar, Academia Militar, Instituto Universitário Militar, Rua Gomes Freire, 1169-203 Lisbon, Portugal

8 Transport Phenomena Research Center (CEFT), Faculdade de Engenharia da Universidade do Porto (FEUP), Rua Roberto Frias, 4200-465 Porto, Portugal

9 Associate Laboratory in Chemical Engineering (ALiCE), Faculty of Engineering, University of Porto, 4200-465 Porto, Portugal

q	Heat (W)
q''	Heat flux (W m^{-2})
Q	Volumetric flow rate (mL min^{-1})
Re	Reynolds number (–)
T	Temperature (°C)
v	Velocity (m s^{-1})
W_{ch}	Channel width (mm)
W_p	Distance between channels (mm)

Greek letters

α	Thermal diffusivity (mm^2 s^{-1})
μ	Viscosity (mPa s)
ρ	Density (kg m^{-3})

Subscripts

exp	Experimental
f	Fluid
in	Inlet
m	Medium
out	Outlet
Petukhov	Petukhov
s	Surface

Introduction

Composites are materials formed by the combination of a matrix, which can be polymeric, metallic, or ceramic, with a dispersed phase made up of particles, fibres, or other types of reinforcement to achieve improved or new properties that were not present in each component individually. Within this context, polydimethylsiloxane (PDMS), an elastomeric polymer, is highly suitable to produce composites.

PDMS exhibits good chemical stability [1] and interesting mechanical properties, such as elasticity [2] and tensile strength [3], excellent optical transparency [4], and its fabrication process is simple, carried out by replica moulding [5]. It is compatible with both metallic [6] and polymeric moulds made of, for instance, polylactic acid (PLA) [7] and acrylonitrile butadiene styrene (ABS) [8].

During the PDMS fabrication process, there is a liquid phase, which consists of the liquid polymer combined with a curing agent [5]. Before solidifying, this liquid phase allows for the incorporation of particles, facilitating the creation of composites. Although PDMS is a material with a low thermal conductivity of around 0.16 W m^{-1} K^{-1} at 25 °C [9], adding particles with higher conductivities can enhance its thermal capacity [10–13]. However, even with the addition of particles, PDMS-based materials still exhibit a thermal conductivity ranging from 0.7 to 3 W m^{-1} K^{-1}, which is lower than the thermal conductivity of, for example, polyethylene [14, 15].

According to Damle et al. [16], many thermal management systems used for electronics cooling are made of copper and silicon. However, the intrinsic rigidity of these materials, combined with their high thermal and electrical conductivities, poses challenges in creating flexible cooling systems with direct contact and a more effective performance. Furthermore, according to the same authors, PDMS is a promising alternative due to its low density, thermal stability, chemical inertia, and electrical insulating properties. These characteristics make it an ideal material for fabricating lightweight thermal management systems with direct contact with electronics. Additionally, the flexibility and ease of fabrication of PDMS open opportunities for developing technologies that are applicable not only to foldable electronics but also to systems in microgravity and electric motors.

In line with this reasoning, Du et al. [17] emphasize the advantage of using PDMS in thermal interface materials due to its relatively superior heat transfer performance, as well as its good elasticity, as previously stated by Damle et al. [16]. Compared to other polymers, they stress the fundamental importance of studying the thermal transfer mechanisms of PDMS to improve its conductivity and meet the ever-increasing requirements of electronic devices.

Research on the thermal conductivity of PDMS with different embedded materials has already revealed significant advancements. One study [18] achieved a thermal conductivity of 7.46 W m^{-1} K^{-1} using boron nitride nanosheets at 15.8 vol %, which is considered a low volumetric concentration of particles. Furthermore, the study maintained the structural flexibility of the PDMS, allowing for repeated bending and twisting after the formation of the composite [18]. Various methods, formulations, particle morphologies, and surface treatments have been investigated to enhance the thermal conductivity of the PDMS composites. In this particular, solutions with elevated particle loadings and moderate particle sizes have recently shown some beneficial features [12, 19–21].

Recently, Jang et al. [22] developed a foldable hybrid sheet using a PDMS matrix filled with copper flakes and silicon carbide (SiC) powder, designed for applications in semiconductors, electronics, and the automotive industry. The results demonstrated high thermal conductivity that enhanced heat dissipation and provided shielding against electromagnetic interference (EMI). In the study, the authors used an acrylate resin as an adhesive containing graphene and hexagonal boron nitride (h-BN), which improved the thermal dissipation. Additionally, the material exhibited excellent flexibility and strength, withstanding over 300,000 bending test cycles without microfractures.

In 2021, Du et al. [17] conducted a molecular dynamics analysis to investigate the factors influencing heat transfer enhancement in pure PDMS. They concluded that longer PDMS chains promote better heat transfer, with amorphous PDMS exhibiting higher thermal conductivity than

crystalline PDMS due to its more stable structure and greater density.

Studies involving flow in PDMS focus on microfluidics, with special emphasis on microchannels. These microchannels are widely used to manipulate small volumes of fluid, directing interest toward the dynamic behaviour of fluids at microscopic scales. The precise control of flow in these systems has driven significant advances in microfluidic devices [23], particularly in biomedical engineering [5] and microelectromechanical systems (MEMS) [24]. However, these studies often underexplored aspects such as heat transfer characteristics and pressure drop. Some works have addressed these issues, but still at the microscale, such as the study by Jung et al. [25], which investigated variations in velocity and temperature fields to examine the effect of heat sinks with microchannels on heat transfer using μPIV and μLIF techniques. Another example is the study by Maia et al. [26], which analysed the heat transfer performance in microchannels with working fluids such as distilled water and nanofluids based on alumina (Al_2O_3) and iron oxide (Fe_3O_4). However, these analyses remain necessary on larger scales like those addressed in this work.

Within this context, to gain a better understanding of heat transfer at the macroscale in both pure PDMS and composites based on it, three types of heat exchangers were tested in this work: one made of pure PDMS, a second comprising PDMS with the addition of recycled graphite, and a third using PDMS and commercial aluminium nanoparticles as filler. The thermal performance analysis was conducted by measuring the thermal conductivity of the materials. In order to evaluate the heat transfer capability, serpentine-type heat exchangers were developed and subjected to forced flow of deionized water (DI-Water) in a single-phase regime with an imposed heat flux. Finally, an infrared thermographic camera was used to obtain the temperature distribution on the heating surface.

The results showed that, although the recycled graphite particles were not on a nanometric scale as their average grain size is inferior to 4 μm, they exhibited superior thermal conductivity and better thermal performance during the DI-Water flow compared to the aluminium nanoparticles. These findings not only validate the effectiveness of the used recycled particles in improving composite performance but also promote the development of more sustainable and cost-effective materials with better thermal management ability, thereby expanding their potential applications in electronics and other industries. To further enhance the thermal performance of PDMS and PDMS-composite heat exchangers, future studies should investigate the use of nanofluids (*e.g.*, graphene, Al_2O_3, or hybrid nanofluids and green nanofluids) as heat transfer fluids, replacing DI-Water. Such investigations, supported by advanced computational fluid dynamics and experimental validation, could leverage the insights from recent studies on nanofluid heat transfer and modelling [26–33].

Materials and methods

The protocols for the 3D-printed mould preparation and production of the serpentines were followed rigorously to ensure the produced heat exchangers' quality, finish, and precision with carefully chosen slicer settings. The process began with designing and fabricating the moulds, which were created using 3D modelling software, considering the desired dimensions and shapes. PLA was chosen for the mould material due to its low cost and manufacturing fastness. Next, a visual inspection of the 3D-printed moulds was conducted to check for defects, residues or impurities, followed by the cleaning of the surfaces. Subsequently, the PDMS and composite PDMS matrix were prepared by mixing the components uniformly according to the established proportions. The mixture was then poured into the moulds, ensuring uniform filling. Finally, the moulds were placed inside an oven, and a pre-defined minimum curing time was undergone before carefully removing the serpentines from the moulds. More details about these steps are provided in the following points.

Fabrication protocols for the moulds and heat exchangers

The heat exchangers were fabricated using PLA 3D-printed moulds, as mentioned previously. The mould contains an exact inverted replica of the test section that will be studied later. Pure PDMS or PDMS composites were poured into these moulds to manufacture the heat exchanger, following the procedure described below.

For the heat exchanger made from pure PDMS:

(a) Pure PDMS and the curing agent were mixed in a 10:1 ratio to form the base matrix. The mixture was stirred for approximately 5 min with the help of a spatula.
(b) The solution was placed in a vacuum degasser to remove air bubbles.
(c) The mixture was poured into the mould and cured in an oven at 80 °C for 2 h.
(d) The sample was manually removed from the mould using a spatula and mechanical pressure.
(e) After removal, the sample was finished with flush cutters and sanded with sandpaper with different grids.

For the heat exchanger made from pure PDMS + particles (composites):

(f) Particles with the desired mass percentage were added to the base matrix of pure PDMS, as described in (a).
(g) The mixture was manually stirred for 5 min.
(h) The curing agent was added to the PDMS and particle mixture.
(i) The procedure described in (b) was repeated for the mixture.
(j) The composite was poured into the mould and cured in an oven at 80 °C; however, unlike the duration mentioned in (c), the curing was carried out for 48 h.
(k) The same procedure described in (d) was used to remove the sample from the mould.
(l) The same procedure described in (e) was used to finish the sample.

Materials for the heat exchangers and their thermophysical properties

Table 1 contains the data related to the purity grade, brand and CAS number of the materials used in the experiments.

The two types of particles, aluminium and graphite, indicated in Table 1, were the materials used to fabricate the composite heat exchangers. The recycled graphite used in this study comes from residues generated during industrial machining processes, offering a cost-effective and sustainable alternative. The recycled graphite particles had a degree of purity (carbon percentage) superior to 90% and an average grain size inferior to 4 µm. Furthermore, the recycled particles were expected to be cheaper and have thermal performance comparable to the commercially available particles.

After preparing several composite samples containing these recycled particles, it was found that their thermal conductivity was high, as shown below. At this stage, the maximum percentage of graphite that could be used in the production of the heat exchangers was also determined. Preliminary tests showed that particle percentages greater than 30 mass % resulted in the inability of the PDMS to cure.

In order to measure the thermal conductivity, thermal diffusivity, and specific heat per unit volume of the materials, it was used the Hot Disk Thermal Constants Analyzer model TPS 2500S from *Hot Disk*®, which involved the application of a heated flat sensor, known as a hot disk, following the protocol established by the standard ISO 22007-2:2022—*Plastics—Determination of thermal conductivity and thermal diffusivity—Part 2: Transient plane heat source (hot disc)* [27]. The equipment can measure thermal conductivities ranging from 0.005 to 1800 W m^{-1} K^{-1}, with reproducibility generally better than 1% and accuracy exceeding 5%. Further details on the experimental procedure and used components can be found in another work conducted by our research team [34].

To measure the thermophysical properties, the solutions containing either pure PDMS or the two composites were poured into disc-shaped moulds made from PLA via 3D printing, with the same dimensions as those recommended for the equipment's standard reference measurements. After the drying process, the samples were removed from the moulds and taken to the equipment for measurements. Although the TPS 2500S equipment does not require calibration, we conducted a preliminary test using the standard Stainless Steel (AISI 316/316L) block with a known thermal conductivity provided by the equipment manufacturer; this ensured that our test conditions were in accordance with the reference and yielded results within the margin of error indicated in the user manual. The results of this validation test are presented in Table 2, including the measured value and the associated uncertainty.

It is important to note that PDMS is considered a thermal insulator with significantly lower thermal conductivity than stainless steel. Consequently, the test conditions used for the standard block are not necessarily applicable to PDMS. For instance, the Hot Disk sensor emits a heat pulse over a specific period, and the pulse amplitude, penetration depth, and duration vary depending on the thermal response of the test material. Therefore, we performed a dedicated test using a pure PDMS specimen to define appropriate test parameters. These adjusted conditions were then used consistently for the composite samples as well. Further details can be found in another work by the group [35]. The main results are summarized in Table 3.

Table 2 Measured thermophysical properties of the standard block (Stainless Steel AISI 316/316L) used as a reference for calibration

Property	Measured value	Standard deviation/%
Thermal conductivity	13.89 W m^{-1} K^{-1}	0.06
Thermal diffusivity	3.700 mm^2 s^{-1}	0.27
Heat capacity	3.754 MJ m^{-3} K^{-1}	0.33

Table 1 Purity grade, brand and CAS number of the materials used in the experiments

Product	Degree of purity	Brand	CAS
184 Silicone Elastomer Base (PDMS)	–	SYLGARD	GMID: 01673921
184 Silicone Elastomer Curing Agent	–	SYLGARD	GMID: 01673921
Aluminium (38 nm)	99.995%	Nanografi	7429-90-5
Graphite waste*	> 90%	DEM's Workshop	–

Table 3 Measured thermophysical properties of the samples

Samples	k/W m^{-1} K^{-1}	α/mm^2 s^{-1}	c_p/MJ m^{-3} K^{-1}
PDMS	0.1954	0.1544	1.258
PDMS + Aluminium 30 mass %	0.2935	0.2044	1.438
PDMS + Graphite 30 mass %	0.5215	0.2524	2.072

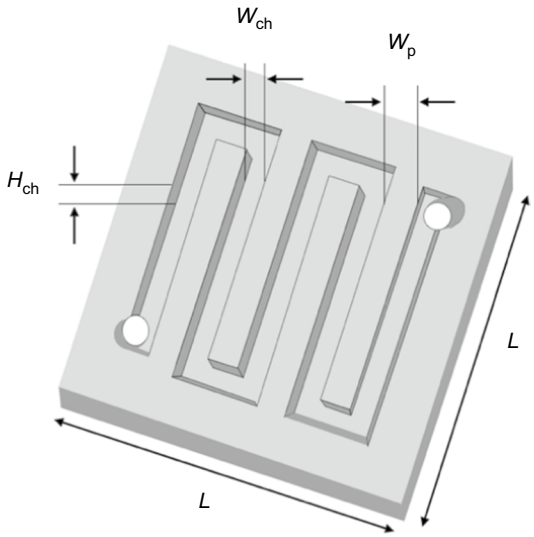

Fig. 1 Schematic design with the dimensions of the PDMS serpentines

Geometry of the heat exchangers

For all the PDMS test sections analysed, the lengths (L) were 65 mm, the channel width (W_{ch}) was 5 mm, the channel height (H_{ch}) was 5 mm, and the distance between channels (W_p) was 6.3 mm. Figure 1 shows a schematic of the nominal dimensions of the PDMS serpentine, and Fig. 2 presents real images of the heat exchangers.

Experimental setup and uncertainties

For the single-phase flow tests, using DI-Water as the working fluid, the experimental setup, as shown in Fig. 3, comprised a peristaltic pump Model NE-9000 for pumping the liquid, a test section heated by a thin stainless steel sheet (electric resistance), storage reservoir, power supply *Axio Met*® AX-3020L 20VDC 20A DC responsible for inducing the heat flow in the stainless steel sheet, a digital multimeter *PCWork*® used to measure the actual power supplied to the resistance, a data acquisition board DT9829 DAQ responsible for recording the inlet and outlet fluid temperatures measured by type-T thermocouples, wall temperature type-K thermocouple, and pressure measurement via pressure transducer *Omega Dyne*® PX409-005 DWUV powered by a second power supply *Leybold*® 521 45, a thermographic camera *Onca*® MWIR-InSb-320 for obtaining the temperature values distribution on the heated surface, and finally, a computer for data storage.

Figure 4 shows the test section positioned on a flat wooden plate with a circular hole of 10 mm diameter that allows the capture of images by the thermographic camera. Directly above the wooden plate, the electrical resistance, a 20 µm thick AISI 304 stainless steel foil, with the same dimensions of 65 mm × 65 mm as the PDMS heat exchanger, is positioned. The PDMS serpentine is placed on top of the electrical resistance, with the flow channel facing downwards, meaning that the liquid passing through the heat exchanger also contacts the electrical resistance. Finally, an acrylic piece is screwed onto the wooden plate, and the mechanical pressure from the tightening of the screws ensures complete sealing of the system.

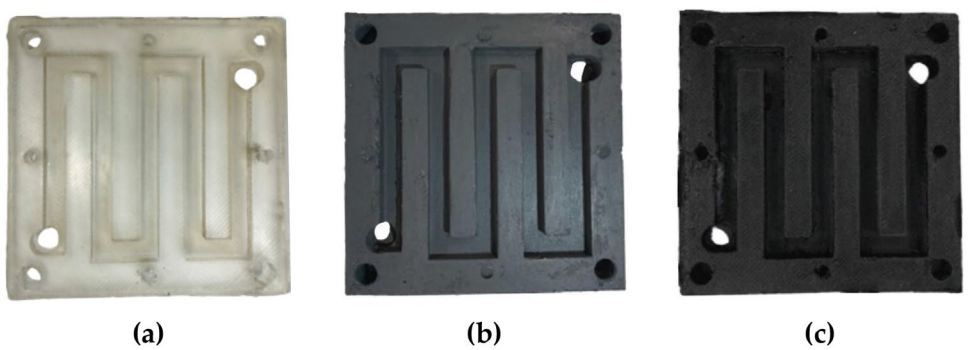

Fig. 2 Real images of the PDMS serpentines. **a** Pure PDMS; **b** Composite with PDMS + Aluminium 30 mass. %; **c** Composite with PDMS + Graphite 30 mass %

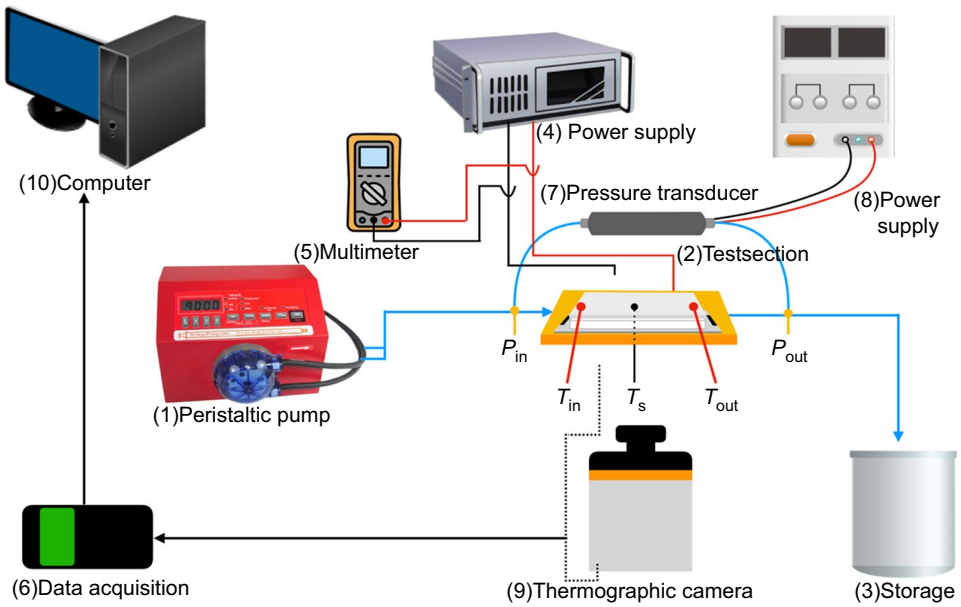

Fig. 3 Scheme of the experimental apparatus used in the flow tests. (1) Peristaltic pump, (2) test section, (3) fluid storage, (4) power supply for the test section resistance, (5) digital multimeter, (6) data acquisition, (7) pressure transducer, (8) power supply of the pressure transducer, (9) thermographic camera, (10) computer

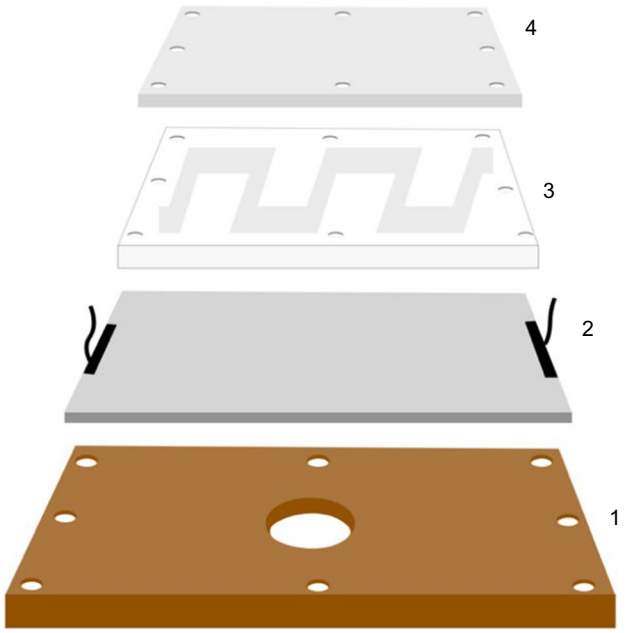

Fig. 4 Details of the test section positioned on a flat wooden plate (1) wooden board with a circular hole, (2) heating surface and electrical connections, (3) heat exchanger, (4) Acrylic piece to fix all the elements to the wooden board

The heat flux is applied to the electrical resistance through the Joule effect. A type-T thermocouple measured the wall temperature of the test section. It was placed below the electrical resistance, secured with thermal paste and positioned at the edge of the central hole so as not to obstruct the thermographic camera's view. The temperature recorded by this thermocouple was used in the thermal heat transport equations mentioned in this study.

The thermographic camera (Onca® MWIR-InSb-320), equipped with a 14-bit analog-to-digital converter, recorded the surface temperature distribution by assigning Analog-to-Digital Units (ADUs) based on radiation intensity. An integration time of 400 µs was set to prevent pixel saturation within the operating temperature range, as validated in [32, 36]. The thermocouple values also served as a reference for calibrating the thermographic camera. It is essential to note that the side of the stainless steel foil facing the thermal camera was coated with high-temperature-resistant black paint to enhance emissivity ($\varepsilon = 0.98$, as per the manufacturer), ensuring accurate and consistent temperature readings. Also, the thermal camera captured only the radiation emitted by the external surface of the painted stainless-steel foil. The PDMS and the working fluid were not directly visible to the camera; their thermal influence was indirectly assessed through temperature variations on the foil surface. For the thermographic analysis, the temperature gradients of the heated surface were obtained once the flow reached the steady-state regime. The complete calibration procedure and data treatment can be found in [36].

To estimate the uncertainty of the dependent variables, we employed the method outlined by Line and McClintock, as described by Figliola and Beasley [37] through Eq. (1):

$$u = \pm \sqrt{\left(\sum_{i=1}^{n} \theta_i u_{Xi} \right)^2} \tag{1}$$

In this equation, u represents the absolute uncertainty of the dependent variable, θ_i denotes the first partial derivative and u_{Xi} indicates the uncertainty of the independent variables. For certain equipment, such as the power supply and peristaltic

pump, the uncertainties provided by the manufacturers were considered and presented in Table 4. The uncertainties for the thermocouples were assessed following the guidelines from the Guide to the Expression of Uncertainty in Measurement (GUM) [38].

Data reduction

Pressure drop

The theoretical single-phase liquid pressure drop is calculated using Eq. (2), provided in the sequence:

$$\Delta p = \frac{2 f_{\text{app}} \rho L v^2}{D_{\text{h}}} \tag{2}$$

where f_{app} is the friction factor for hydrodynamically developing laminar flow, as given by Shah and London [39] and adjusted by the equation from Churchill and Usagi [40]. The friction factor f_{app}, which encompasses both developing and fully developed single-phase regions, was experimentally derived by Copeland [41],

$$f_{\text{app}}\text{Re} = \left\{ \left[3.2\left(L^{+}\right)^{-0.57} \right]^2 + (f\text{Re})^2 \right\}^{1/2} \tag{3}$$

where L^{+} represents the distance along the channel in the hydrodynamic entrance region, expressed as a dimensionless axial coordinate:

$$L^{+} = \frac{L}{\text{Re} D_{\text{h}}} \tag{4}$$

and f is the friction factor for fully developed laminar flow, given by:

$$f\text{Re} = 19.64G + 4.7 \tag{5}$$

with G is a function of the channel aspect ratio, defined as:

Table 4 Experimental uncertainties

Equipment/Variable	Uncertainty
Peristaltic pump NE-9000, Q	±3%
Axio Met® AX-3020L 20VDC 20A DC, i	±0.05 A
PCWork® digital multimeter, i	±0.05 A
Omega® PX409-005DWUV Differential pressure sensor, p	±0.28 kPa
Leybold® 521 45 power supply, V	±0.05 V
Serpentine parameters, L, H_{ch}, W_{ch}, W_{p}	±0.05 mm
Thermal conductivity, k	±5 %
Type-K and type-T thermocouples, T	±0.30 °C

$$G = \left[\left(W_{\text{ch}}/H_{\text{ch}} \right)^2 + 1 \right] / \left[\left(\left(W_{\text{ch}}/H_{\text{ch}} \right) + 1 \right)^2 \right] \tag{6}$$

Heat transfer parameters

The electrical resistance connected to the power source provides effective heat to the liquid inside the flow channel, which is given by:

$$q = \dot{m} c_{\text{p}} \left(T_{\text{f,out}} - T_{\text{f,in}} \right) \tag{7}$$

where $\dot{m}$ represents the mass flow rate in kg s^{-1}, c_{p} is the specific heat capacity of the liquid in J kg^{-1} K^{-1}, $T_{\text{f,out}}$ and $T_{\text{f,in}}$ are, respectively, the liquid's average outlet and inlet temperatures in the test section. So, the heat flux in the test section was calculated as follows:

$$q'' = \frac{q}{A_{\text{eff}}} = \frac{\dot{m} c_{\text{p}} \left(T_{\text{f,out}} - T_{\text{f,in}} \right)}{wL} \tag{8}$$

where w and L are the width and the length of the liquid flow channel, both in meters. In order to determine the experimental heat transfer coefficient, h_{exp}, it was used the following expression:

$$h_{\text{exp}} = \frac{q''}{\left(T_{\text{s}} - T_{\text{m,f}} \right)} \tag{9}$$

where T_{s} ,represents the wall temperature and $T_{\text{m,f}} = \frac{T_{\text{in,f}} + T_{\text{out,f}}}{2}$ is the average temperature of the fluid.

Nusselt number

The experimentally obtained Nusselt number can be given by:

$$Nu_{\text{exp}} = \frac{h_{\text{exp}} D_{\text{h}}}{k_{\text{f}}} \tag{10}$$

where D_{h} represents the hydraulic diameter of the flow channel in meters and k_f represents the thermal conductivity of the fluid in W m^{-1} K^{-1}, obtained by considering the average liquid temperature.

To compare the experimental results with correlations from the literature, Petukhov's correlation [42] was selected, as this equation accounts for thermally developing laminar flow. Additionally, the correlation relates the fluid viscosity, μ_f, obtained considering the average temperature of the flowing fluid, with the viscosity at the surface temperature, μ_s. Petukhov's correlation [42] is expressed as follows:

$$\text{Nu}_{\text{Petukhov}} = 1.55 \left(\frac{\text{RePr} D_{\text{h}}}{L} \right)^{0.33} \left(\frac{\mu_{\text{f}}}{\mu_{\text{s}}} \right)^{0.14} \tag{11}$$

where Re represents the Reynolds number, and Pr is the Prandtl number.

It is important to note that surface roughness effects were not explicitly considered when determining the heat transfer coefficient. Since all the PDMS and composite heat exchangers were fabricated using identical 3D-printed moulds and underwent the same curing and finishing protocols, the surface characteristics remained consistent across samples. This ensured that any observed variations in thermal performance could be primarily attributed to material properties rather than geometric or surface differences.

Results and discussion

Fluid flow characteristics

The pressure sensor used in our experimental setup could not measure the variations in the pressure drop, as the instrument's uncertainty was greater than the acquired values. For this reason, these data were not considered for the analysis. Our flow system or serpentine can be classified as a macrochannel (defined by a hydraulic diameter equal to or greater than 5 mm). Additionally, the volumetric flow rates (5, 10, and 15 mL min^{-1}) are extremely low, resulting in an almost negligible pressure drop. Thus, we used a correlation from the literature to analyse the pressure drop, as shown in Fig. 5. In this sense, we adopted Copeland's correlation [41], as it accounts for various effects that may occur during flow, considering both geometric parameters of the channel and inlet flow conditions.

The results obtained from the Copeland model show a similar trend in the curves for the three serpentines tested. The two composite surfaces exhibit a slightly lower pressure drop than pure PDMS, although these differences can be neglected. A similar trend was observed in [34]'s experimental study, where the authors found no significant difference in pressure drop between pure PDMS and PDMS/hBN nanocomposite in a staggered micro-pin fin arrangement. A completely uniform dispersion of nanoparticles/microparticles in the polymeric matrix of PDMS may justify these results, keeping the friction factor practically unchanged among the different serpentines tested. However, in the future, it is essential to conduct experimental measurements of the pressure drop in the system to confirm the trend shown by the theoretical model.

Heat transfer parameters

DI-Water, with a fixed initial temperature, flows over the heated surface. As it moves, it absorbs heat from the wall, resulting in an increase in its temperature. At the end of the flow, the difference between the initial and final temperatures of the DI-Water indicates the amount of heat absorbed from the surface. Therefore, a greater variation between these temperatures reflects higher heat transfer efficiency. Figure 6 illustrates this effect for the three exchangers tested experimentally. The results show that the composite heat exchangers provide a more efficient heat transfer, absorbing more heat from the heated surface than the pure PDMS exchanger.

To explain this effect, we refer to Table 3, presented in section "Materials for the heat exchangers and their thermophysical properties", which shows the thermophysical properties of the surfaces. Adding particles to the PDMS matrix increases the thermal conductivity, which is the primary factor responsible for the increased heat transfer. Both composites exhibit similar values for an imposed volumetric flow rate of 5 mL min^{-1}, with about a 2 °C difference compared to pure PDMS. However, as the flow rate increases, the PDMS + 30 mass % aluminium composite tends to approach the values of pure PDMS, while the PDMS + 30

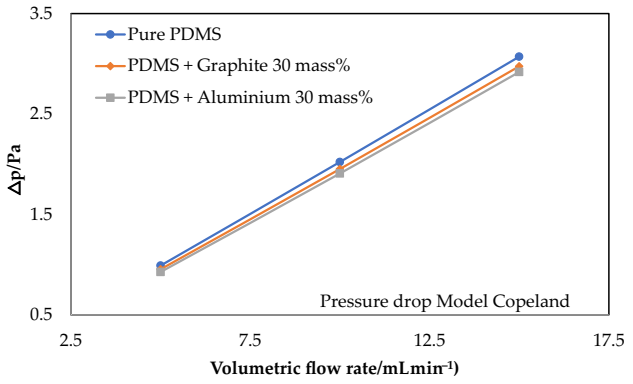

Fig. 5 Pressure drop verified in the pure PDMS, PDMS + 30 mass % graphite, and PDMS + 30 mass % aluminium serpentines

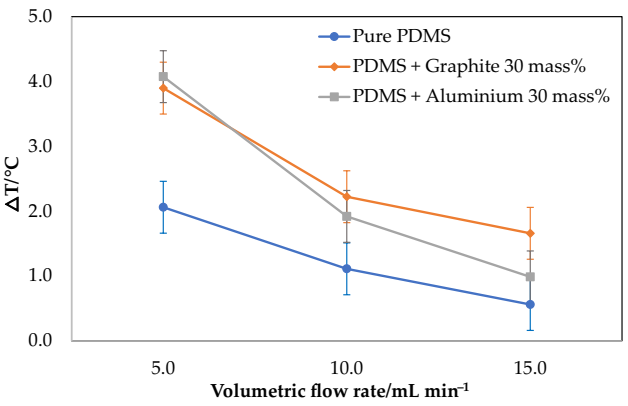

Fig. 6 Temperature difference between inlet and outlet as a function of volumetric flow rate for pure PDMS, PDMS + 30 mass % graphite, and PDMS + 30 mass % aluminium

mass % graphite composite maintains a significant difference, demonstrating superior thermal capacity.

The heat transfer coefficient for PDMS and composites is shown in Fig. 7. The curves indicate that the composite devices exhibit a higher heat transfer coefficient compared to pure PDMS. As explained earlier, the increase in thermal conductivity provided by adding particles to the PDMS matrix is the main factor responsible for these results. For volumetric flow rates of 5 and 10 mL min^{-1}, the heat transfer coefficient is, on average, 2.5 times higher in the composites compared to pure PDMS. For a volumetric flow rate of 15 mL min^{-1}, the composite with graphite particles is up to 2 times more efficient than the aluminium composite and ~ 5 times more efficient than pure PDMS.

The obtained thermographic images help us better understand the heat transfer coefficient values. Figure 8 shows the temperature distribution profiles for the three different heat exchangers analysed in this study, considering the same volumetric flow rate. The central region in the images represents the flow channel of DI-Water in the serpentine, while the upper and lower extremities show the temperature distribution of the walls of the heat exchangers.

Analysing the images from left to right, it is observed that the first surface, composed solely of PDMS, Fig. 8a, reveals that the material maintains its essential characteristic as a thermal insulator. Heat exchange is concentrated in the central region, indicating that the PDMS prevents uniform thermal energy dissipation to other regions beyond the liquid in the flow channel, preserving its insulating nature even under the higher volumetric flow rates (up to 15 mL min^{-1}) imposed in this work.

In the composite surfaces, thermal exchanges also occur on the sides of the heat exchangers, resulting in a more uniform temperature distribution, as shown in Fig. 8c more clearly. Heat in this region is transferred by conduction due to the increased thermal conductivity provided by the addition of particles to the PDMS matrix. The higher the thermal conductivity of the particle used—in this case, graphite—the greater the heat dissipation capability of the material.

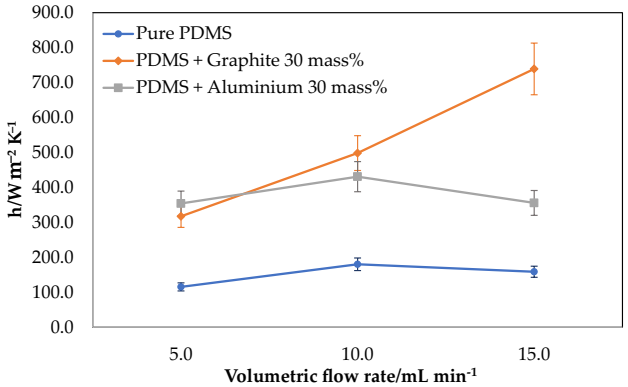

Fig. 7 Heat transfer coefficient as a function of the volumetric flow rate for pure PDMS, PDMS + 30 mass % graphite, and PDMS + 30 mass % aluminium

Nusselt number

Figure 9 presents the experimentally obtained Nusselt numbers as a function of the Reynolds number. The figure also presents the curves determined by Petukhov's correlation [42] for comparison purposes. This correlation considers a laminar flow regime and thermally developing conditions. Additionally, it includes a term that relates the viscosity of the liquid at the average flow temperature to the viscosity of the liquid if it were at the same temperature as the surface. This adjustment is particularly important when changing the type of material on the heated surface, as is the case with the present research study. Different materials can influence the wall's temperature and, consequently, the liquid's viscosity and heat transfer efficiency.

The comparison between the results provided by Petukhov's correlation and those obtained experimentally reveals a significant difference in the Nusselt number. Only for the pure PDMS surface are the experimental results lower than those predicted by the correlation, as shown in Fig. 9a. This trend is reversed for the composites, as illustrated in Fig. 9b and c. It is also worth noticing that the composite formed by graphite and PDMS shows a consistent experimental increase in the Nusselt number as the Reynolds number

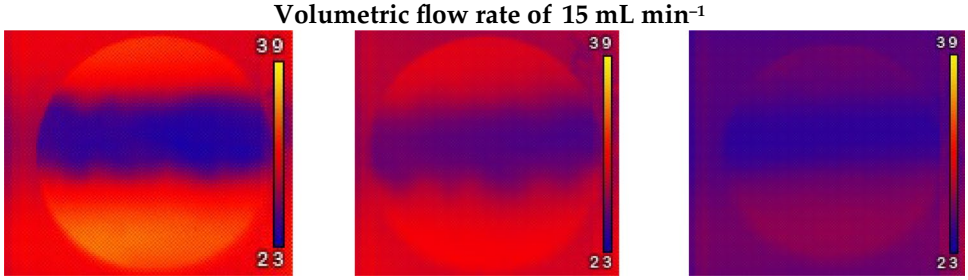

(a) DI-Water in PDMS (b) DI-Water in PDMS+Aluminium (c) DI-Water in PDMS+Graphite

Fig. 8 Thermographic images of the temperature distribution profile for the three examined heat exchangers at a 15 mL min^{-1} volumetric flow rate

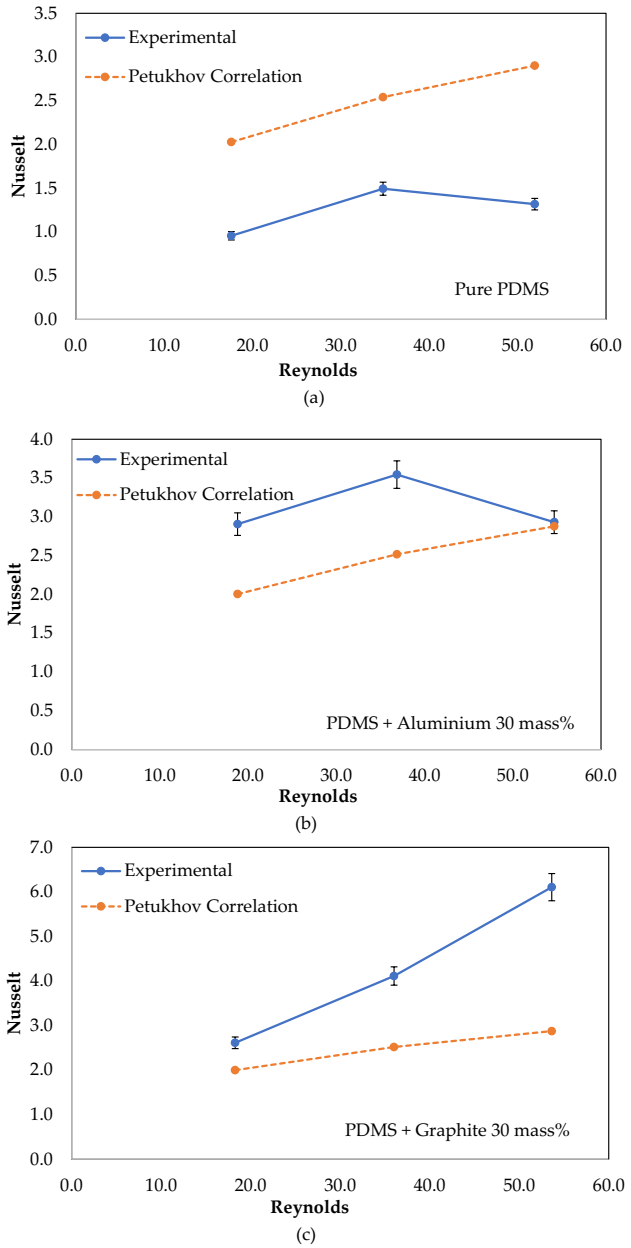

Fig. 9 Experimental Nusselt number values versus Petukhov's correlation [42]

increases, with the impact being more substantial at the maximum flow rate.

Conclusions and recommendations for future studies

This study evaluated the thermal performance of three distinct heat exchangers of different materials: pure PDMS, PDMS matrix with commercially available aluminium nanoparticles, and PDMS matrix with recycled graphite. The goal was to investigate the efficiency of these materials in terms of heat transfer, pressure drop, and temperature distribution using a thermographic imaging camera while also validating the use of recycled particles as a sustainable and economical alternative to commercial ones. The key findings are summarized in the following topics:

- With the addition of recycled graphite particles and aluminium nanoparticles, PDMS composites showed significant improvement in thermal conductivity compared to pure PDMS. The PDMS with recycled graphite exhibited the highest thermal conductivity, nearly 3 times greater than pure PDMS.
- The addition of particles to the composites resulted in greater heat transfer efficiency. For volumetric flow rates of 5 and 10 mL min^{-1}, the heat transfer coefficients of the composites were, on average, 2.5 times higher than those of pure PDMS. In the case of the graphite composite, the performance was up to 5 times superior.
- Thermal imaging analysis indicated that the composites allowed for more uniform temperature distribution. In composite surfaces, the heat was transferred not only in the serpentine channel but also along the sides of the heat exchangers, highlighting the positive effect of the increased thermal conductivity of the composites.
- The PDMS composite with recycled graphite serpentine maintained superior performance even with increased flow rates, proving to be more thermally efficient than the aluminium composite serpentine.
- Due to the lack of references in the literature on pressure drop in PDMS-based composite materials, future experimental studies dealing with this will be most welcome to confirm the existing theoretical trends and to achieve better knowledge on the subject.
- Because of the few published studies using heat exchangers made of composite materials with recycled waste particles, further experimental works should be conducted to test the heat transfer performance of composite-based heat exchangers with recycled fillers.
- Future studies should also include environmental durability tests, such as thermal cycling, prolonged exposure to humidity, and mechanical stress analysis, to assess the reliability and sustainability of these materials for real-world applications.
- While this study focused on demonstrating the technical feasibility and thermal performance of recycled graphite particles in PDMS composites, a detailed cost-performance assessment was not performed. Considering the promising thermal results obtained with low-cost recycled materials, future works should address a comprehensive techno-economic analysis and investigate these composites' scalability and industrial integration potential. Particular attention should be given

to challenges such as maintaining consistent material properties during large-scale manufacturing, ensuring uniform particle dispersion, and adapting the fabrication process for integration with existing commercial heat exchanger technologies.

Overall, thermal conductivity measurements and volumetric flow rate results confirmed that the composite surfaces can be effectively used in cooling systems to enhance their thermal performance. Also, one of the most significant contributions of this work lies in the use of low-cost yet thermally efficient recycled particles.

Acknowledgements The authors are grateful to the Fundação para a Ciência e a Tecnologia (FCT), Avenida D. Carlos I, 126, 1249–074 Lisboa, Portugal, for partially financing the Project "Estratégias interfaciais de arrefecimento para tecnologias de conversão com elevadas potências de dissipação", Ref. PTDC/EMETED/7801/2020). José Pereira acknowledges FCT for his PhD Fellowship (Ref. 2021. 05830.BD). The authors are also grateful for FCT funding through 2022.03151. PTD (https://doi.org/10.54499/2022.03151.PTDC), 2022.06207.PTDC (https://doi.org/10.54499/2022.06207.PTDC) and LA/P/0083/2020 IN +-IST-ID. The authors also acknowledge the partial financial support within the R&D Units Project Scope: UIDB/04077/2020, UIDP/04077/2020 (UID/4077: Mechanical Engineering and Resource Sustainability Center (MEtRICs)),. Glauco Nobrega was supported by the PRT/BD/153088/2021 doctoral grant financed by the Portuguese Foundation for Science and Technology (FCT), and with funds from MCTES/República Portuguesa, under the MIT Portugal Program. Inês S. Afonso was supported by the doctoral grant 2024.05919.BDANA, financed by FCT. A.S. Moita also acknowledges FCT for partially financing her contract through CEECINST/00043/2021/CP2797/CT0005, https://doi.org/10.54499/CEECINST/00043/2021/CP2797/CT0005 and for supporting Mr. Pedro Ponte's PhD fellowship (Ref. SFRH/BD/149286/2019). E.M. Cardoso is grateful for the financial support from Conselho Nacional de Desenvolvimento Científico e Tecnológico (grants number 458702/2014–5, 309848/2020–2 and 309848/2020-2) and Fundação de Amparo à Pesquisa do Estado de São Paulo (grants numbers 2013/15431–7, 2019/02566–8, 2023/03492-3, 2023/14537-8, 2022/03946–1 and 22/15765–1).

Authors' contributions Reinaldo Souza: Writing—original draft, Methodology, Investigation, Conceptualization, Formal analysis, Data curation, Project administration. Glauco Nobrega: Writing—review & editing, Writing—original draft, Supervision, Software, Methodology, Formal analysis, Data curation, Conceptualization. Inês Afonso: Investigation, Formal analysis, Data curation. José Pereira: Writing—review & editing, Writing—original draft, Investigation. Elaine Cardoso: Writing—review & editing, Supervision, Methodology. Filipe Marques: Writing—original draft, Validation, Investigation, Formal analysis, Conceptualization. Cândida Vilarinho: Writing—review & editing, Validation, Supervision. Ana Moita: Writing—review & editing, Supervision, Resources, Project administration, Methodology. Rui Lima: Conceptualization, Funding acquisition, Methodology, Project administration, Resources, Supervision, Writing—review & editing.

Funding Open access funding provided by FCT|FCCN (b-on).

Declarations

Conflict of interest There is no conflict of interest in publishing our paper in your esteemed journal.

Ethical approval The entire work is the original work.

Consent for publication All the authors have given their consent to publish the paper.

References

1. ML van P, Zhou F FAU—Ramstedt M, Ramstedt M FAU—Hu L, Hu L FAU—Huck WTS, WT H. A self-assembly approach to chemical micropatterning of poly(dimethylsiloxane). PG—6634-7 FAU—van Poll, Maaike L. Melville Laboratory for Polymer Synthesis, Department of Chemistry, University of Cambridge, Lensfield Road, Cambridge CB2 1EW, UK. FAU—Zhou, Feng.
2. Wang Z, Volinsky AA, Gallant ND. Crosslinking effect on polydimethylsiloxane elastic modulus measured by custom-built compression instrument. J Appl Polym Sci. 2014;131(22):41050.
3. Zhang G, Sun Y, Qian B, Gao H, Zuo D. Experimental study on mechanical performance of polydimethylsiloxane (PDMS) at various temperatures. Polym Test. 2020;90:106670.
4. Lee S, Shin H-J, Yoon S-M, Yi DK, Choi J-Y, Paik U. Refractive index engineering of transparent ZrO_2–polydimethylsiloxane nanocomposites. J Mater Chem. 2008;18(15):1751–5. https://doi.org/10.1039/B715338D.
5. Miranda I, Souza A, Sousa P, Ribeiro J, Castanheira EMS, Lima R, et al. Properties and applications of PDMS for biomedical engineering: a review. J Funct Biomater. 2022;13:2.
6. Yousuff CM, Danish M, Ho ET, Kamal Basha IH, Hamid NHB. Study on the optimum cutting parameters of an aluminum mold for effective bonding strength of a PDMS microfluidic device. Micromachines. 2017;8:258.
7. van der Borg G, Warner H, Ioannidis M, van den Bogaart G, Roos WH. PLA 3D printing as a straightforward and versatile fabrication method for PDMS molds. Polymers. 2023;15:1498.
8. Iuliano A, van der Wal E, Ruijmbeek CWB, Groen SLM, Pijnappel WWMP, de Greef JC, et al. Coupling 3D printing and novel replica molding for in-house fabrication of skeletal muscle tissue engineering devices. Adv Mater Technol. 2020;5(9):2000344. https://doi.org/10.1002/admt.202000344.
9. Zhang Z, Liao M, Li M, Li L, Wei X, Kong X, et al. Enhanced thermal conductivity for polydimethylsiloxane composites with core-shell CFs@SiC filler. Compos Commun. 2022;33:101209.
10. Han B, Chen H, Hu T, Ye H, Xu L. High electrical conductivity in polydimethylsiloxane composite with tailored graphene foam architecture. J Mol Struct. 2020;1203:127416.
11. Timbs K, Khatamifar M, Antunes E, Lin W. Experimental study on the heat dissipation performance of straight and oblique fin heat sinks made of thermal conductive composite polymers. Therm Sci Eng Prog. 2021;22:100848.

12. Mi H-Y, Jing X, Huang H-X, Turng L-S. Novel polydimethylsiloxane (PDMS) composites reinforced with three-dimensional continuous silica fibers. Mater Lett. 2018;210:173–6.
13. Linshuang Long LW. Structured polydimethylsiloxane (PDMS) composite with enhanced thermal and radiative properties for heat dissipation. J Enhanc Heat Transf. 2021;28(4):79–93.
14. Henry A, Chen G. Anomalous heat conduction in polyethylene chains: theory and molecular dynamics simulations. Phys Rev B. 2009;79(14):144305. https://doi.org/10.1103/PhysRevB.79.144305.
15. Henry A, Chen G. High thermal conductivity of single polyethylene chains using molecular dynamics simulations. Phys Rev Lett. 2008;101(23):235502. https://doi.org/10.1103/PhysRevLett.101.235502.
16. Damle N, Joshi Y. Experimental and analytical study of the hydrodynamic and single and two-phase convective heat transfer performance of flexible PDMS microchannels with micropillar arrays. Appl Therm Eng. 2023;224:119799.
17. Du Y, Liu S, Yuan S, Zhang H, Yuan S. A study of influence factors to improve the heat transfer of pure-polydimethylsiloxane (PDMS): a molecular dynamics study. Colloids Surfaces A Physicochem Eng Asp. 2021;618:126409.
18. Hou X, Chen Y, Lv L, Dai W, Zhao S, Wang Z, et al. High-thermal-transport-channel construction within flexible composites via the welding of boron nitride nanosheets. ACS Appl Nano Mater. 2019;2(1):360–8. https://doi.org/10.1021/acsanm.8b01939.
19. Gao BZ, Xu JZ, Peng JJ, Kang FY, Du HD, Li J, et al. Experimental and theoretical studies of effective thermal conductivity of composites made of silicone rubber and Al_2O_3 particles. Thermochim Acta. 2015;614:1–8.
20. Cheng C, Liu F, Yang HK, Xiao K, Xue C, Yang S-T. High-performance n-butanol recovery from aqueous solution by pervaporation with a PDMS mixed matrix membrane filled with zeolite. Ind Eng Chem Res. 2020;59(16):7777–86. https://doi.org/10.1021/acs.iecr.9b06104.
21. Wei J, Liao M, Ma A, Chen Y, Duan Z, Hou X, et al. Enhanced thermal conductivity of polydimethylsiloxane composites with carbon fiber. Compos Commun. 2020;17:141–6.
22. Jang D-H, Kim T-W, Kim Y-D, Han K-Y. A hybrid sheet of nanofiller/PDMS composite with thermal dissipation and EMI shielding properties for foldable displays. J Inf Disp. 2024;25(3):243–50. https://doi.org/10.1080/15980316.2023.2285731.
23. Zhou J, Ellis AV, Voelcker NH. Recent developments in PDMS surface modification for microfluidic devices. Electrophoresis. 2010;31(1):2–16. https://doi.org/10.1002/elps.200900475.
24. Ashraf MW, Tayyaba S, Afzulpurkar N. Micro electromechanical systems (MEMS) based microfluidic devices for biomedical applications. Int J Mol Sci. 2011;12:3648–704.
25. Jung SY, Park JH, Lee SJ, Park H. Heat transfer and flow characteristics of forced convection in PDMS microchannel heat sink. Exp Therm Fluid Sci. 2019;109:109904.
26. Maia I, Rocha C, Pontes P, Cardoso V, Miranda JM, Moita AS, et al. Heat transfer and fluid flow investigations in pdms microchannel heat sinks fabricated by means of a low-cost 3D printer. In: Ren Y, editor. Rijeka: IntechOpen; 2020. p. Ch. 8. https://doi.org/10.5772/intechopen.89735
27. Murtaza S, Kumam P, Sutthibutpong T, Suttiarporn P, Srisurat T, Ahmad Z. Fractal-fractional analysis and numerical simulation for the heat transfer of $ZnO+Al_2O_3+TiO_2$/DW based ternary hybrid nanofluid. ZAMM J Appl Math Mech / Zeitschrift für Angew Math und Mech. 2024;104(2): e202300459. https://doi.org/10.1002/zamm.202300459.
28. Murtaza S, Kumam P, Ahmad Z, Ramzan M, Ali I, Saeed A. Computational simulation of unsteady squeezing hybrid nanofluid flow through a horizontal channel comprised of metallic nanoparticles. J Nanofluids. 2023;12:1327–34.
29. Murtaza S, Ali F, Sheikh NA, Khan I, Nisar KS. Analysis of silver nanoparticles in engine oil: Atangana–Baleanu fractional model. Comput Mater Contin. 2021;67:2915–32.
30. Memon AA, Murtaza S, Memon MA, Bhatti K, Haque M, Ali MR. Simulation of thermal decomposition of calcium oxide in water with different activation energy and the high Reynolds number. Complexity. 2022;2022(1):3877475. https://doi.org/10.1155/2022/3877475.
31. Ullah I, Ali F, Mohamad Isa S, Murtaza S, Jamshed W, Eid MR, et al. Electro-magnetic radiative flowing of Williamson-dusty nanofluid along elongating sheet: Nanotechnology application. Arab J Chem. 2023;16(5):104698.
32. Nobrega G, Souza R, Cardoso B, Afonso I, Pereira J, Cardoso E, et al. Experimental evaluation of green nanofluids in heat exchanger made oF PDMS. Therm Sci Eng Prog. 2024;55:102978.
33. Murtaza S, Kumam P, Ahmad Z, Sitthithakerngkiet K, Sutthibutpong T. Fractional model of Brinkman-type nanofluid flow with fractional order Fourier's and Fick's Laws. Fractals. 2023;31(10):2340199. https://doi.org/10.1142/S0218348X23401990.
34. Cardoso EM, de Souza RR, Correa RGM, Utsab Banerjee SKM. Heat transfer and fluid flow in PDMS nanocomposite micro-pin fin heat sinks. In: 10th World Conference on Experimental Heat Transfer, Fluid Mechanics and Thermodynamics 26–30 August 2024, Rhodes Island, Greece. 2024.
35. Pereira J, Souza R, Moreira A, Moita A. Durable and high-temperature-resistant superhydrophobic diatomite coatings for cooling applications. Coatings. 2024;14:805.
36. Teodori E, Pontes P, Moita AS, Moreira ALN. Thermographic analysis of interfacial heat transfer mechanisms on droplet/wall interactions with high temporal and spatial resolution. Exp Therm Fluid Sci. 2018;96:284–94.
37. Figliola RS, Beasley DE. Theory and design for mechanical measurements. 4th ed. TA - TT -. New York SE - xvi, 542 pages : illustrations ; 26 cm + 1 card (13 x 13 cm): Wiley; 2006.
38. GUM, Bureau International Des Poids Et Mesures; Organization Internationale De Normalisation-Guide to the expression of uncertainty in measurement. International Organization for Standardization. 2008.
39. Shah RK, London AL. Chapter V—circular duct. In: Shah RK, London ALBT-LFFC in D, editors. Academic Press; 1978. pp. 78–152. Available from: http://www.sciencedirect.com/science/article/pii/B9780120200511500103
40. Churchill SW, Usagi R. A general expression for the correlation of rates of transfer and other phenomena. AIChE J. 1972;18(6):1121–8. https://doi.org/10.1002/aic.690180606.
41. Copeland D. Optimization of parallel plate heatsinks for forced convection. In: Sixteenth Annual IEEE Semiconductor Thermal Measurement and Management Symposium (Cat No00CH37068). 2000. pp. 266–72.
42. Petukhov BS. Heat transfer and friction in turbulent pipe flow with variable physical properties. In: Hartnett JP, Irvine TFBT-A in HT, editors. Elsevier; 1970. p. 503–64. Available from: https://www.sciencedirect.com/science/article/pii/S0065271708701539